

Ab initio investigation of electron capture by Cl^{7+} ions from H

L. B. Zhao¹, Ayako Watanabe², P. C. Stancil¹, and M. Kimura³

¹*Department of Physics and Astronomy and Center for Simulational Physics,
University of Georgia, Athens, Georgia, 30602-2451, USA*

²*Information, media and education square,
Ochanomizu University, Tokyo, 112-8610 Japan and*

³*Graduate School of Sciences, Kyushu University, Fukuoka 812-8581, Japan*

(Dated: March 23, 2007)

Abstract

An investigation of charge transfer in collisions of ground-state Cl^{7+} with H has been conducted, based on a fully quantum-mechanical molecular-orbital close-coupling (QMOCC) approach. The charge-transfer process $\text{Cl}^{7+}(^1\text{S}) + \text{H} \rightarrow \text{Cl}^{6+}(2p^6nl\ ^2\text{S},\ ^2\text{P}^o,\ ^2\text{D},\ ^2\text{F}^o,\ ^2\text{G}) + \text{H}^+$ with $n = 5$ and 6 is taken into account for collision energies between 10^{-4} eV/u and 1 keV/u. The relevant adiabatic potentials and nonadiabatic coupling matrix elements for the ClH^{7+} system are evaluated with the configuration-interaction method. The investigation shows that electron capture into the $5d$, $5f$, $5g$ and $6p$ states dominate for collision energies less than ~ 1 eV/u, while above 100 eV/u the $5s$, $5p$, $5d$, and $6p$ are the primary capture channels. Comparison with experimental data for collisions of $\text{Cl}^{7+}(^1\text{S})$ with D reveals a discrepancy over the full range of measured energies (5-430 eV/u), while no significant isotope effect is found for QMOCC calculations with deuterium. Furthermore, comparison with a previous calculation on the one-electron $\text{N}^{7+} + \text{H}$ system as well as measurements on the multielectron $\text{Al}^{7+} + \text{H}$ and $\text{Fe}^{7+} + \text{H}$ systems suggests the electronic structure of the core has a non-negligible effect on the charge-transfer process. A one-electron model for relative l -distributions is found to agree with the QMOCC results for $n = 5$ between 100-1000 eV/u, but fails at lower collision energies. Finally, state-selective and total rate coefficients are given for temperatures between 10 and 200,000 K.

PACS numbers: 34.20.Mq, 34.50.-s, 34.70.+e

I. INTRODUCTION

Charge transfer, or electron capture, in ion-atom and ion-molecule collisions has attracted researchers' attentions for decades because of its application importance in laboratory and astrophysical plasmas [1, 2]. Depending on physical conditions, such as temperature and density, charge transfer reactions may play a crucial role in establishing the ionization balance of the plasmas and may significantly contribute to ion emission spectra by populating excited states of ions. Recent theoretical analyses of x-ray and extreme ultraviolet emission spectra from some comets have confirmed that charge transfer is a major excitation mechanism and is responsible for the major portion of the observed emission [3]. Since many astronomical bodies, such as comets, planetary nebulae, supernova remnants, and the sun, are too far away to be probed directly, line emission from astronomical objects is frequently used as a diagnostic of their composition and physical properties (see, e.g., [4–6]).

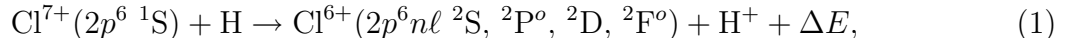
In addition to its importance in the practical applications mentioned above, understanding the dynamics of ion-atom and ion-molecule collisions is also one of the major driving forces for investigations of charge transfer. Such studies provide useful information on molecular structure and interactions in ion-atom and ion-molecule systems. This can be accomplished through comparison of measured and calculated charge-transfer cross sections. The comparisons are also useful to check the validity of classical, semiclassical, and quantal theories describing the collision problems [7] and their valid ranges.

To date, significant progress has been made in laboratory studies of charge transfer (see, e.g., [3]). A great deal of experimental work has been conducted, including measurements of total and state-selective cross sections for exchange of one or more electrons, and detailed, n - and ℓ -resolved line emission spectra for a variety of ion-atom and ion-molecule systems. Many theoretical approaches, such as quantal and semiclassical molecular-orbital close-coupling [8, 9], atomic-orbital close-coupling [10], classical trajectory Monte Carlo [11], and continuum distorted wave methods [12], have been developed to describe charge transfer processes. Applications of these theoretical approaches to individual collisional systems have been reviewed in Ref. [3].

Although electron capture by many ions from atoms or molecules have been reported, both experimental and theoretical data for capture by *heavy* multicharged ions with multielectron cores are relatively scarce. Experimentally, this is partly due to the difficulty

in making sufficiently intense beams at low collision energies [13]. Recently, absolute total integral cross sections for electron capture in collisions of Cl^{7+} with atomic deuterium were measured at the Oak Ridge National Laboratory ion-atom merged-beams apparatus, but no *ab initio* study was performed for the system [13]. Only a fully quantal molecular-orbital close-coupling hidden-crossing calculation was performed for the same charged $\text{N}^{7+} + \text{D}$ system for comparison. The comparison was satisfactory over the energy range 4.6 – 140 eV/u. Even so, the experiment showed contradiction to the prediction from a simple multi-channel Landau-Zener model for Cl^{7+}/D , and to measurements for other multicharged (7+) ions with multielectron cores: Fe^{7+} [14] and Al^{7+} [15].

In the present paper, we perform an *ab initio* investigation of electron capture by Cl^{7+} from H by utilizing a fully quantal molecular-orbital close-coupling (QMOCC) approach. The concerned charge transfer reactions are



with $n = 3, 4, 5, 6,$ and 7 . In Sec. II, calculations of the molecular potentials and nonadiabatic radial and rotational coupling matrix elements for the ClH^{7+} system are described, while Section III briefly surveys the QMOCC scattering theory. In Sec. IV, state-to-state, state-selective n - and ℓ -resolved, and total cross sections and rate coefficients are presented and compared to available measurements and calculations. Section V summarizes the main results. Atomic units are used unless otherwise specified.

II. MOLECULAR STRUCTURE CALCULATIONS

The adiabatic potential energy curves and nonadiabatic radial and rotational coupling matrix elements essential to the current collision calculations are obtained with the configuration-interaction method using the quantum chemistry package *ALCHEMY*. Details about the *ALCHEMY* package can be found in Refs. [16, 17]. Here we only outline its application to the current problem. The frozen-core approximation is adopted in the calculation. The ten electrons in the 3σ and 1π orbitals are frozen, while one electron in 36σ , 25π , 16δ orbitals is treated as active. Slater-type orbitals (STOs) are employed for the atomic basis set. For the chlorine atom, all orbitals up to the $n = 5$ manifold are included, while a restricted set of orbitals are considered for $n = 6-8$. All orbitals up to $n = 2$ are

considered for the hydrogen atom [18]. The Slater exponents are given in Table I.

The adiabatic potentials for all molecular electronic states corresponding to the asymptotic limits $\text{Cl}^{6+}(2p^6n\ell) + \text{H}^+$ with $n = 3, 4, 5, 6,$ and 7 and $\ell = s, p, d, f,$ and $g,$ and $\text{Cl}^{7+}(2p^6) + \text{H},$ and nonadiabatic radial and rotational coupling matrix elements between these states were calculated from internuclear distance $R = 0.5$ to 29 a.u. The calculated asymptotic energies are presented for the twenty $^2\Sigma^+$ and ten $^2\Pi$ molecular states relative to the $\text{Cl}^{7+}(2p^6\ ^1\text{S}) + \text{H}$ channel and compared with experimental asymptotic atomic energies [19] in Table II. The maximum relative error of the current results from the experimental data is less than 1.94%. Because the entrance channel $\text{Cl}^{7+}(2p^6\ ^1\text{S}) + \text{H}$ forms only one $^2\Sigma$ state, the $^2\Delta$ states corresponding to $\text{Cl}^{6+}(2p^6n\ell) + \text{H}$ contribute to the charge-transfer reactions (1) only by a two-step rotational coupling interaction, first coupled with $^2\Pi$ and then with $^2\Sigma$. Thus their contribution is expected to be small and therefore are neglected.

In Fig. 1, the adiabatic potential energies (solid curves) are plotted as a function of internuclear distance R for the thirteen molecular states considered in the scattering calculations. The eight $^2\Sigma^+$ and five $^2\Pi$ potentials curves are given in (a) and (b), respectively. Thus only transitions from the 15 $^2\Sigma^+$ state to 8 $^2\Sigma^+$, 9 $^2\Sigma^+$, 6 $^2\Pi$, 10 $^2\Sigma^+$, 7 $^2\Pi$, 11 $^2\Sigma^+$, 8 $^2\Pi$, 12 $^2\Sigma^+$, 9 $^2\Pi$, 13 $^2\Sigma^+$, 14 $^2\Sigma^+$, and 10 $^2\Pi$ are taken into account. Thirty eight nonadiabatic radial couplings and forty rotational couplings are involved in the current calculations. Test calculations using a larger set of molecular states, as given in Table II, found the capture cross sections to the remaining states to be negligible for the considered energy range. Those states correlating to the $n = 3$ and 4 manifolds have very short-range interactions and will only contribute for energies greater than ~ 10 keV/u, while the states correlating to $6d, 6f, 6g,$ and the $n = 7$ manifold have very long-range avoided-crossings with the entrance channel and can be considered completely diabatic. In Figs. 2 and 3, nine representative nonadiabatic radial couplings and eight representative rotational couplings are plotted as a function of R . The potentials have been transformed from the adiabatic representation to the diabatic representation. The diagonal diabatic potential energies (dashed curves) are illustrated in Fig. 1 and representative off-diagonal matrix elements are given in Fig. 4. We will discuss how the diabatic potentials are obtained in the next section.

Beyond $R = 29.0$ a.u., the potentials for the entrance channels are described by the

charge-induced-dipole interactions

$$V_L(R) = -\frac{\alpha_d}{2R^4} + E_\infty, \quad (2)$$

where α_d is the dipole polarizability of neutral H and E_∞ is the separated-atom energy. All the quantities in Eq. (2) are in atomic units (a.u.). For all the exit channels, the long-range potentials ($R > 29.0$ a.u.) are Coulombic. E_∞ is determined using the α_d parameter and the *ab initio* potentials.

III. SCATTERING THEORY

A quantal molecular-orbital close-coupling (QMOCC) approach to describe electron capture in ion-atom collisions has been formulated by Kimura and Lane [8] and Zygelman *et al.* [9]. Here only a brief summary of its main theoretical aspects and formulae is given.

QMOCC involves solving a coupled set of second-order differential equations. Its solutions are the expansion coefficients, or scattering amplitudes, of the total system wave function expanded over a truncated set of adiabatic molecular eigenfunctions. In the adiabatic representation, transitions from a molecular state to another molecular state are driven by the vector potential $A(\mathbf{R})$, where \mathbf{R} is the coordinate of the relative nuclear motion. However, it is numerically more convenient to perform the scattering calculations in a diabatic representation which can be obtained with a unitary transformation. By making the unitary transformation, the set of the coupled equations in the diabatic representation is given by

$$-\frac{1}{2\mu}\nabla^2 G(\mathbf{R}) + U(R)G(\mathbf{R}) = EG(\mathbf{R}), \quad (3)$$

where μ is the nuclear reduced mass of the ion-atom pair, E is the relative collision energy in the center-of-mass frame, $G(\mathbf{R})$ is the scattering amplitude describing relative motion of the nuclei, and $U(R)$ with $R = |\mathbf{R}|$ is the diabatic potential matrix whose off-diagonal elements are responsible for driving charge transfer in the diabatic representation, defined by

$$U(R) = W(R)[V(R) - P(R)]W^{-1}(R), \quad (4)$$

where $V(R)$ is a diagonal matrix with elements consisting of adiabatic eigenvalues for each channel state, $W(R)$ is the unitary matrix that obeys the equation

$$\frac{dW(R)}{dR} + iW(R)A^{rad}(R) = 0, \quad (5)$$

and $P(\mathbf{R})$ is a coupling matrix whose elements are given by [20, 21]

$$P_{\alpha\beta} = \mp \frac{1}{\mu R^2} [(J \mp \Lambda_\alpha)(J \pm \Lambda_\alpha + 1)]^{1/2} A_{\alpha\beta}^{rot} \delta(\Lambda_\alpha, \Lambda_\beta \mp 1), \quad (6)$$

where J is the total angular momentum, Λ is the component of electronic angular momenta along the internuclear axis, and $A^{rad}(R)$ and $A^{rot}(R)$ are, respectively, the radial and rotational components of the vector potential $[A(\mathbf{R})]_{\alpha\beta} = i\langle\psi_\alpha|\nabla_{\mathbf{R}} + \sum_k f(\mathbf{r}_k; \mathbf{R})\nabla_{\mathbf{r}_k}|\psi_\beta\rangle$ with ψ_α and ψ_β being the adiabatic electronic eigenfunctions. The second term in the vector potential is due to the introduction of an electron translation factor (see for example Refs. [17, 22]) where \mathbf{r}_k is the coordinate for electron k and $f(\mathbf{r}_k; \mathbf{R})$ is a so-called switching function defined as in Watanabe *et al.* [17]. The introduction of the translation factor ensures that all asymptotic radial and rotational couplings go to zero even for dipole-connected asymptotic atomic states as seen in Figs. 2 and 3.

By introducing a partial-wave decomposition for $G(\mathbf{R})$, Eq. (3) can be further simplified. The resulting set of radial coupled equations may be solved with the log-derivative method of Johnson [23]. From the numerical results of the log-derivative and the asymptotic expressions of the radial functions, the K matrix may be extracted and thus the scattering matrix S is obtained

$$S_J = [I + iK_J]^{-1}[I - iK_J]. \quad (7)$$

Finally the charge transfer cross sections from channel α to channel β is expressed in terms of the scattering matrix elements

$$\sigma_{\alpha\rightarrow\beta} = \frac{\pi g_\alpha}{k_\alpha^2} \sum_J (2J + 1) |(S_J)_{\alpha\beta}|^2, \quad (8)$$

where k_α denotes the wave number for center-of-mass motion of the initial ion-atom channel, and g_α is an approach probability factor of the initial channel α .

IV. RESULTS AND DISCUSSION

A thirteen-channel close-coupling calculation was performed using the molecular electronic structure and coupling data in Sec. II. Eight states of the thirteen channels are of symmetry $^2\Sigma^+$ and five states of symmetry $^2\Pi$. Only electron capture into 6ℓ with $\ell = s$ and p and all 5ℓ orbitals of Cl^{6+} ($2p^6n\ell$) is included. The contributions from the individual partial waves are summed as in Eq. (8) until a convergence of the cross sections is achieved.

Since the speed of convergence depends on the relative collision energy, the computations are satisfactorily fast for low energy, but become prohibitively lengthy above a few 100 eV/u because of the increase in the number of partial waves.

State-to-state cross sections are illustrated in Figs. 5. (a) and (b) corresponding, respectively, to capture into the ${}^2\Sigma^+$ states via radial coupling and into the ${}^2\Pi$ states through rotational coupling from the entrance channel $15\ {}^2\Sigma^+$. Figure 5 shows that capture into the $10\ {}^2\Sigma^+$, $11\ {}^2\Sigma^+$, $12\ {}^2\Sigma^+$, $13\ {}^2\Sigma^+$ and $14\ {}^2\Sigma^+$ states is dominant below 0.1 eV/u. This is easily interpreted from Fig. 1(a) where the avoided-crossings of the adiabatic potentials of these states and the entrance channel is seen in the large R (> 10 a.u.) range. The avoided-crossings correspond to sharp peaks of the radial couplings in Fig. 2(a), such as at $R = 18.3$ and 22.0 a.u. This illustrates that there exists strong couplings among these channels, while the strong couplings result in the dominant charge-transfer transitions. It should be emphasized that we used Lorentzian profiles to replace the three largest radial couplings at $R = 12.8$, 18.3 and 22.0 a.u. to prevent unphysical oscillations in the interpolation of the couplings in the sharp avoided-crossing regions. Above about 0.1 eV/u, charge transfer due to rotational coupling such as $15\ {}^2\Sigma^+ \rightarrow 6\ {}^2\Pi$, $7\ {}^2\Pi$ and $10\ {}^2\Pi$ begins to become important and is comparable to that due to radial coupling at 10.0 eV/u. This is because the possibility for the system to penetrate the inner region with small and intermediate R becomes larger with increasing collision energy, while stronger couplings between the molecular states occur for $R < 10.0\ a_0$ as seen in Fig. 3.

To get an insight into the dominant physical processes, Thompson *et al.* [13] performed a multichannel Landau-Zener analysis of the diabatic potentials for ClD^{7+} and suggested that capture into the $4d$ and $4f$ states dominated charge transfer in the 20 to 1000 eV/u energy range and that the $5s$ state begins to contribute to the cross sections below 20 eV/u. Although such a conclusion, which depends on the form of the adopted empirical couplings [13], was found to agree qualitatively with a fully quantal molecular-orbital close-coupling hidden-crossing (FQ-MOCC-HC) theoretical analysis for the ND^{7+} system, it is different from our computational results for the ClH^{7+} system. The current QMOCC and potential calculations show that the contributions from electron capture into the 3ℓ , 4ℓ , $6d$, $6f$, $6g$, and 7ℓ orbitals are negligible. In order to compare the contribution from capture into the 5ℓ , $6s$ and $6p$ orbitals involved in the current calculation, the state-selective cross sections are plotted in Fig. 6. It is seen that the $5d$, $5f$, $5g$ and $6p$ dominate the charge-transfer processes

over the entire energy range considered and the $5s$ and $5p$ begin to become important only above a few eV/u. The $6s$ is seen to be only important at energies less than 10^{-3} eV.

An empirical ℓ -distribution function for charge transfer reactions was proposed by Abramov *et al* [24] and widely utilized in plasma modeling [3]. However, few theoretical examinations of such a distribution have been made. Here we check the validity of the ℓ -distribution function by comparing with our *ab initio* QMOCC results. The function is written in the form

$$W_{n\ell} = (2\ell + 1) \frac{[(n - 1)!]^2}{(n + \ell)!(n - 1 - \ell)!}. \quad (9)$$

This equation is explicitly independent of collision energy, but thought to be suitable for the low-energy range below 1 keV/u. Furthermore, it is strictly relevant to single-electron systems, but has been widely, and usually incorrectly, adopted for multielectron ions [3]. In Fig. 7, the Abramov *et al.* distribution function $W_{n\ell}$ for $n = 5$ is plotted along with our *ab initio* QMOCC results at $E = 1, 10, 100,$ and 1000 eV/u. The comparison shows a strong energy dependence for the ℓ -distribution with the Abramov *et al.* function being reasonably accurate for 100-1000 eV/u, but failing for smaller collision energies. This suggests that care must be exercised when using empirical distribution functions particularly when the energy range of applicability is not clearly defined. Furthermore, it is expected that as the collision energy exceeds 10 keV/u, the ℓ -levels should be populated by a statistical distribution given by

$$W_{n\ell}^{\text{st}} = (2\ell + 1)/n^2. \quad (10)$$

The QMOCC results displayed in Fig. 7, suggest that even up to as high as 1 keV/u, the ℓ -distribution for Cl^{7+}/H is far from statistical.

The total QMOCC charge transfer cross section due to collisions of Cl^{7+} with H are compared with the measured cross sections for the $\text{Cl}^{7+} + \text{D}$ system and theoretical cross sections for the $\text{N}^{7+} + \text{D}$ system in Fig. 8 [13]. An obvious discrepancy is seen between the current QMOCC calculations and the measurement. In the low energy range, the discrepancy may be attributed to the kinematic isotope effect, which was found to be very significant for charge transfer between N^{4+} and H(D) [25]. However, it has been shown that in the higher energy range, such as for collision energies greater than ~ 50 eV/u, the H and D cross sections become quantitatively indistinguishable. The current QMOCC cross sections are higher than the measured cross sections approximately by a factor of two above

~ 50 eV/u. To ensure that the difference with experiment is not due to an isotope effect, we performed additional calculations using the $\text{Cl}^{7+} + \text{D}$ reduced mass in Eq. (3) for energies between 0.5 and 100 eV/u. As shown in Fig. 8, the results are practically identical to the $\text{Cl}^{7+} + \text{H}$ calculation.

Although the molecular-orbital close-coupling hidden-crossing calculation seems to support the experimental data, such a support may be weak because it assumes that effects of the closed [Ne] core are negligible without a theoretical examination. In contrast to such an assumption, a comparison between the FQ-MOCC-HC calculation and the current QMOCC results suggests that the electronic structure of the closed [Ne] shell has a significant effect on the electron capture cross sections. Such a result might be expected by considering the potential energies given in Fig. 1, where interaction with the [Ne] core removes the degeneracy in the Cl^{6+} $n = 5$ and 6 manifolds, unlike in the hydrogen-like N^{6+} case. For example, the avoided-crossing for the N^{6+} $n = 5$ state occurs near 11.5 a.u. [13], while for the Cl^{6+} $n = 5$ manifold, the avoided-crossings for each individual ℓ -channel are spread out between ~ 8 and 13 a.u. Furthermore, from Fig. 8, a hint of this core interaction is evident in the experimental results for $\text{Fe}^{7+}(4s) + \text{H} \rightarrow \text{Fe}^{6+}(4snl) + \text{H}^+$ [14] and $\text{Al}^{7+}(2p^2) + \text{H} \rightarrow \text{Al}^{6+}(2p^2nl) + \text{H}^+$ [15], which have larger total cross sections than the measured Cl^{7+}/D or calculated N^{7+}/D cases.

Rate coefficients are evaluated by averaging the QMOCC cross sections in Fig. 6 (a) and (b) over a Maxwellian velocity distribution. The results are tabulated in Table III. The temperature ranges from 10 to 2.0×10^5 K. For convenience, the rate coefficients are fitted to the form

$$\alpha(T) = \sum_i a_i \left(\frac{T}{10,000} \right)^{b_i} \exp \left(-\frac{T}{c_i} \right), \quad (11)$$

where α is the rate coefficient in cm^3/s , and T is temperature in K. The fitting parameters, a_i (cm^3/s), b_i , and c_i (K), are given in Table IV. In the temperature range considered, the fits do not deviate from the computed rate coefficients by more than 24.2%, 16.2%, 16.6%, 9.7%, 7.0%, 0.7%, 5.0%, and 3.0% for electron capture into the $5s$ ^2S , $5p$ $^2\text{P}^o$, $5d$ ^2D , $5f$ $^2\text{F}^o$, $5d$ ^2G , $6s$ ^2S , and $6p$ $^2\text{P}^o$ states of $\text{Cl}^{6+}(2p^6nl)$, and the summed exit channels, respectively.

V. SUMMARY

Charge transfer has been investigated for collisions of Cl^{7+} and H, based on the quantal molecular-orbital close-coupling approach. The configuration interaction (ALCHEMY) method is used to evaluate the molecular electronic structure and coupling matrix elements between the adiabatic molecular states for the ClH^{7+} system. Cross sections are presented for electron capture into the exit channels $\text{Cl}^{6+}(2p^6n\ell) + \text{H}$ channels for collisions of $\text{Cl}^{7+}(2p^6\ ^1S)$ with H for collision energies between 0.1 meV/u and 1 keV/u. Rate coefficients are given for temperatures between 10 K and 2.0×10^5 K. The current QMOCC investigation shows that electron capture into $5d$, $5f$, $5g$ and $6p$ states dominate the cross section for collision energies less than 1 eV/u, while above 100 eV/u the $5s$, $5p$, $5d$, and $6p$ are the primary capture channels. Comparison with the experimental data for collisions of $\text{Cl}^{7+}(^1S)$ and D reveal a large discrepancy, even for energies greater than ~ 50 eV/u where kinematic isotope effects are believed to be negligible [25]. Furthermore, we also compared the current QMOCC results with the fully quantal molecular-orbital hidden-crossing cross sections for the $\text{N}^{7+} + \text{D}$ system as well as with the measurements for the same charged $\text{Fe}^{7+} + \text{H}$ and $\text{Al}^{7+} + \text{H}$ systems. This accumulated evidence suggests that the electronic structure of the core has a non-negligible effect on the charge transfer process. Further experimental investigations for collisions of Cl^{7+} with H (D) and for other multielectron ions are needed.

Acknowledgments

L.B.Z. and P.C.S. acknowledge support from NASA Grant No. NNG05GD98G and NSF Grant No. INT-0300708, and M.K. from the Ministry of Education, Science, Sport, Culture and Technology, Japan Society for Promotion of Science (JSPS) for the US-JP Collaborative Research Program, and Collaborative Research Grant by National Institute for Fusion Science.

-
- [1] R. K. Janev, Review of Fundamental Processes and Applications of Atoms and Ions (World Scientific, Singapore, 1993).
- [2] G. J. Ferland, Annu. Rev. Astron. Astrophys. **41**, 517 (2003).

- [3] V. A. Krasnopolsky, J. B. Greenwood, and P. C. Stancil, *Space Sci. Rev.* **113**, 271 (2004), and references therein.
- [4] C. M. Lisse, D. J. Christian, K. Dennerl, K. J. Meech, R. Petre, H. A. Weaver, and S. J. Wolk, *Science* **292**, 1343 (2001).
- [5] F. P. Keenan, C. A. Ramsbottom, K. L. Bell, K. A. Berrington, A. Hibbert, W. A. Feibelman, and W. P. Blair, *Astrophys. J.* **438**, 500 (1995).
- [6] A. D. Silber, S. F. Anderson, B. Margon, and R. A. Downers, *Astrophys. J.* **462**, 428 (1996).
- [7] J. Caillat, A. Dubois, I. Sundvor, and J.-P. Hansen, *Phys. Rev. A* **70**, 32715 (2004).
- [8] M. Kimura and N. F. Lane, *Adv. At. Mol. Phys.* **26**, 79 (1990).
- [9] B. Zygelman, D. L. Cooper, M. J. Ford, A. Dalgarno, J. Gerratt, and M. Raimondi, *Phys. Rev. A* **46**, 3846 (1992).
- [10] W. Fritsch, *Phys. Rev. A* **35**, 2342 (1987); W. Fritsch and C. D. Lin, *Phys. Rep.* **202**, 1 (1991).
- [11] R. Abrines and I. C. Percival, *Proc. Phys. Soc. Lond.* **88**, 861 (1966); R. E. Olson and A. Salop, *Phys. Rev. A* **16**, 531 (1977).
- [12] Dž. Belkić, R. Gayet and A. Salin, *Phys. Rep.* **56**, 279 (1979).
- [13] J. S. Thompson, A. M. Covington, P. S. Krstić, Marc Pieksma, J. L. Shinpaugh, P. C. Stancil, and C.C. Havener, *Phys. Rev. A* **63**, 012717 (2000).
- [14] R.A. Phaneuf, *Phys. Rev. A* **28**, 1310 (1983).
- [15] R.A. Phaneuf, M. Kimura, H. Sato, and R.E. Olson, *Phys. Rev. A* **31**, 2914 (1985).
- [16] A. D. McLean, M. Yoshimine, B. H. Lengsfeld, P. S. Bagus, and B. Liu, *ALCHEMY II* (IBM, 1981).
- [17] A. Watanabe, R. Suzuki, H. Sato, and M. Kimura, *Natural Science Report*, Ochanomizu University, vol. 49, No. 2 (1998).
- [18] E. Clementi and C. Roetti, *At Data Nucl. Data Tables* **14**, 177(1974).
- [19] NIST Atomic Spectra Database, website <http://physics.nist.gov/asd>.
- [20] B. H. Bransden and M. R. C. McDowell, *Charge Exchange and the Theory of Ion-Atom Collisions* (Clarendon Press, Oxford, 1992).
- [21] A. R. Turner, D. L. Cooper, J. G. Wang, and P. C. Stancil, *Phys. Rev. A* **68**, 012704 (2003).
- [22] N. Shimakura and M. Kimura, *Phys. Rev. A* **44**, 1659 (1991).
- [23] B. R. Johnson, *J. Comput. Phys.* **13**, 445 (1973).
- [24] V. A. Abramov, F. F. Baryshnikov and V. S. Lisitsa, *JETP Lett.* **27**, 464 (1978).

[25] P. C. Stancil and B. Zygelman, Phys. Rev. Lett. **75**, 1495 (1995).

TABLE I: The STO exponents.

	Cl	H
$1s$	18.0505, 13.3358	$1s$ 1.0
$2s$	7.32724, 5.75219	$2s, 2p$ 0.5
$2p$	10.2877, 5.61299	
$3s$	2.92737, 1.85365	
$3p, 3d$	2.62421, 1.47458	
$4s, 4p, 4d, 4f$	1.9775	
$5s, 5p, 5d, 5f, 5g$	1.5820	
$6s, 6p, 6d, 6f, 6g$	1.318337	
$7s, 7p, 7d, 7f, 7g$	1.130000	
$8s, 8p, 8d, 8f, 8g$	1.108750	

TABLE II: Comparison of asymptotic separated-atom energies (in eV) between the ALCHEMY calculations and experiment for ClH^{7+} . The 38 molecular states are of symmetries ${}^2\Sigma^+$ and ${}^2\Pi$.

Asymptotic atomic state	Mol. state	This work	Expt. ^a
$\text{Cl}^{6+}(2p^6 3s \ ^2S) + \text{H}^+$	1 ${}^2\Sigma^+$	-99.7719	-100.6026
$\text{Cl}^{6+}(2p^6 3p \ ^2P^o) + \text{H}^+$	2 ${}^2\Sigma^+$	-84.6436	-85.1952
	1 ${}^2\Pi$	-84.6422	
$\text{Cl}^{6+}(2p^6 3d \ ^2D) + \text{H}^+$	3 ${}^2\Sigma^+$	-64.0412	-64.6201
	2 ${}^2\Pi$	-64.0408	
$\text{Cl}^{6+}(2p^6 4s \ ^2S) + \text{H}^+$	4 ${}^2\Sigma^+$	-42.7737	-43.0736
$\text{Cl}^{6+}(2p^6 4p \ ^2P^o) + \text{H}^+$	5 ${}^2\Sigma^+$	-37.2018	-37.4133
	3 ${}^2\Pi$	-37.1967	
$\text{Cl}^{6+}(2p^6 4d \ ^2D) + \text{H}^+$	6 ${}^2\Sigma^+$	-29.7875	-30.0350
	4 ${}^2\Pi$	-29.7859	
$\text{Cl}^{6+}(2p^6 4f \ ^2F^o) + \text{H}^+$	7 ${}^2\Sigma^+$	-28.1147	-28.1843
	5 ${}^2\Pi$	-28.1142	
$\text{Cl}^{6+}(2p^6 5s \ ^2S) + \text{H}^+$	8 ${}^2\Sigma^+$	-20.1624	-20.3009
$\text{Cl}^{6+}(2p^6 5p \ ^2P^o) + \text{H}^+$	9 ${}^2\Sigma^+$	-17.5044	-17.6088
	6 ${}^2\Pi$	-17.4910	
$\text{Cl}^{6+}(2p^6 5d \ ^2D) + \text{H}^+$	10 ${}^2\Sigma^+$	-13.9801	-14.1099
	7 ${}^2\Pi$	-13.9750	
$\text{Cl}^{6+}(2p^6 5f \ ^2F^o) + \text{H}^+$	11 ${}^2\Sigma^+$	-13.1355	-13.1436
	8 ${}^2\Pi$	-13.1328	
$\text{Cl}^{6+}(2p^6 5g \ ^2G) + \text{H}^+$	12 ${}^2\Sigma^+$	-13.0266	-13.0768
	9 ${}^2\Pi$	-13.0274	
$\text{Cl}^{6+}(2p^6 6s \ ^2S) + \text{H}^+$	13 ${}^2\Sigma^+$	-8.8827	-8.8915
$\text{Cl}^{6+}(2p^6 6p \ ^2P^o) + \text{H}^+$	14 ${}^2\Sigma^+$	-7.4038	-7.4582
	10 ${}^2\Pi$	-7.3766	
$\text{Cl}^{7+}(2p^6 \ ^1S) + \text{H}$	15 ${}^2\Sigma^+$	0.0000	0.0000
$\text{Cl}^{6+}(2p^6 6d \ ^2D) + \text{H}^+$	16 ${}^2\Sigma^+$	-5.4825	-5.5278
	11 ${}^2\Pi$	-5.4688	
$\text{Cl}^{6+}(2p^6 6f \ ^2F^o) + \text{H}^+$	17 ${}^2\Sigma^+$	-5.0138	-4.9679
	12 ${}^4\Pi$	-5.0091	
$\text{Cl}^{6+}(2p^6 6g \ ^2G) + \text{H}^+$	18 ${}^2\Sigma^+$	-4.8323	-4.9278

TABLE III: Rate coefficients for electron capture into the $\text{Cl}^{6+}(2p^6nl\ ^2S, ^2P^o, ^2D, ^2F^o, ^2G) + \text{H}^+$ channels due to $\text{Cl}^{7+}(2p^6\ ^1S) + \text{H}$ collisions. T is in K and the rate coefficients are in cm^3/s . *Total* represents the rate coefficients summed over all the exit channels.

T	$5s\ ^2S$	$5p\ ^2P^o$	$5d\ ^2D$	$5f\ ^2F^o$	$5g\ ^2G$	$6s\ ^2S$	$6p\ ^2P^o$	Total
10	2.18(-14) ^a	2.20(-12)	2.08(-09)	7.65(-10)	7.73(-10)	4.32(-10)	2.79(-09)	6.85(-09)
20	3.80(-14)	2.04(-12)	2.02(-09)	9.03(-10)	7.02(-10)	4.28(-10)	2.94(-09)	6.99(-09)
30	5.24(-14)	1.92(-12)	1.93(-09)	9.78(-10)	6.52(-10)	4.23(-10)	2.99(-09)	6.98(-09)
40	6.38(-14)	1.85(-12)	1.86(-09)	1.04(-09)	6.18(-10)	4.21(-10)	3.04(-09)	6.98(-09)
50	7.30(-14)	1.80(-12)	1.79(-09)	1.10(-09)	5.95(-10)	4.21(-10)	3.09(-09)	7.00(-09)
60	8.07(-14)	1.77(-12)	1.74(-09)	1.15(-09)	5.78(-10)	4.21(-10)	3.13(-09)	7.02(-09)
70	8.75(-14)	1.75(-12)	1.70(-09)	1.20(-09)	5.66(-10)	4.22(-10)	3.17(-09)	7.06(-09)
80	9.38(-14)	1.73(-12)	1.66(-09)	1.25(-09)	5.57(-10)	4.23(-10)	3.21(-09)	7.09(-09)
90	9.95(-14)	1.73(-12)	1.62(-09)	1.29(-09)	5.51(-10)	4.25(-10)	3.24(-09)	7.12(-09)
100	1.05(-13)	1.72(-12)	1.59(-09)	1.33(-09)	5.47(-10)	4.26(-10)	3.26(-09)	7.15(-09)
200	1.42(-13)	1.85(-12)	1.37(-09)	1.58(-09)	5.45(-10)	4.42(-10)	3.46(-09)	7.39(-09)
300	1.62(-13)	2.19(-12)	1.28(-09)	1.68(-09)	5.50(-10)	4.55(-10)	3.60(-09)	7.57(-09)
400	1.75(-13)	2.67(-12)	1.25(-09)	1.74(-09)	5.51(-10)	4.66(-10)	3.74(-09)	7.74(-09)
500	1.83(-13)	3.21(-12)	1.25(-09)	1.77(-09)	5.49(-10)	4.76(-10)	3.86(-09)	7.91(-09)
600	1.87(-13)	3.78(-12)	1.28(-09)	1.78(-09)	5.46(-10)	4.86(-10)	3.99(-09)	8.09(-09)
700	1.88(-13)	4.36(-12)	1.32(-09)	1.79(-09)	5.42(-10)	4.96(-10)	4.12(-09)	8.27(-09)
800	1.88(-13)	4.95(-12)	1.36(-09)	1.80(-09)	5.38(-10)	5.05(-10)	4.25(-09)	8.46(-09)
900	1.87(-13)	5.56(-12)	1.41(-09)	1.80(-09)	5.34(-10)	5.14(-10)	4.38(-09)	8.64(-09)
1000	1.86(-13)	6.19(-12)	1.46(-09)	1.79(-09)	5.30(-10)	5.23(-10)	4.51(-09)	8.83(-09)
2000	1.77(-13)	1.57(-11)	2.08(-09)	1.72(-09)	5.03(-10)	5.95(-10)	5.70(-09)	1.06(-08)
3000	2.03(-13)	3.29(-11)	2.73(-09)	1.64(-09)	4.92(-10)	6.50(-10)	6.67(-09)	1.22(-08)
4000	2.70(-13)	5.80(-11)	3.37(-09)	1.57(-09)	4.88(-10)	6.97(-10)	7.49(-09)	1.37(-08)
5000	3.89(-13)	9.17(-11)	3.98(-09)	1.52(-09)	4.88(-10)	7.38(-10)	8.19(-09)	1.50(-08)
6000	5.71(-13)	1.34(-10)	4.56(-09)	1.48(-09)	4.90(-10)	7.76(-10)	8.82(-09)	1.62(-08)
7000	8.29(-13)	1.84(-10)	5.10(-09)	1.44(-09)	4.93(-10)	8.11(-10)	9.37(-09)	1.74(-08)
8000	1.18(-12)	2.42(-10)	5.61(-09)	1.41(-09)	4.96(-10)	8.43(-10)	9.88(-09)	1.85(-08)
9000	1.63(-12)	3.06(-10)	6.10(-09)	1.39(-09)	4.99(-10)	8.74(-10)	1.03(-08)	1.95(-08)
10000	2.21(-12)	3.77(-10)	6.56(-09)	1.37(-09)	5.03(-10)	9.02(-10)	1.08(-08)	2.05(-08)
20000	1.71(-11)	1.30(-09)	1.03(-08)	1.25(-09)	5.43(-10)	1.13(-09)	1.40(-08)	2.85(-08)

TABLE IV: Fitting parameters of rate coefficients for capture into $\text{Cl}^{6+}(2p^6nl\ ^2\text{S},\ ^2\text{P}^o,\ ^2\text{D},\ ^2\text{F}^o,\ ^2\text{G}) + \text{H}^+$ channels, and the summed exit channels (Total) due to $\text{Cl}^{7+}(2p^6\ ^1\text{S}) + \text{H}$ collisions. T is in K; a_i and c_i are in units of cm^3/s and K, respectively.

Param.	$5s\ ^2\text{S}$	$5p\ ^2\text{P}^o$	$5d\ ^2\text{D}$	$5f\ ^2\text{F}^o$	$5g\ ^2\text{G}$	$6s\ ^2\text{S}$	$6p\ ^2\text{P}^o$	Total
a_1	2.5997(-12) ^a	3.9231(-10)	6.5199(-09)	1.0037(-09)	3.4663(-10)	6.3211(-10)	8.4735(-09)	1.4656(-)
b_1	2.9165(+00)	1.9538(+00)	9.6442(-01)	1.3737(-01)	7.8431(-02)	4.7284(-01)	5.9359(-01)	7.0547(-)
c_1	1.0987(+05)	7.7302(+04)	8.3387(+04)	-9.3204(+06)	-2.0014(+05)	2.8849(+05)	1.6200(+05)	2.1728(+)
a_2	1.4413(-12)	1.5820(-12)	4.7009(-10)	2.4833(-09)	1.3895(-10)	2.6759(-10)	2.3249(-09)	5.6402(-)
b_2	5.7480(-01)	-2.7907(-02)	-2.3686(-01)	2.5637(-01)	-1.9133(-01)	-6.1187(-02)	-2.6475(-02)	-3.0024(-)
c_2	1.5419(+03)	-2.3482(+04)	-4.6553(+04)	4.4044(+03)	-1.3881(+05)	-1.1338(+05)	-8.8121(+04)	-9.7076(+)

^a $A(-B) = A \times 10^{-B}$

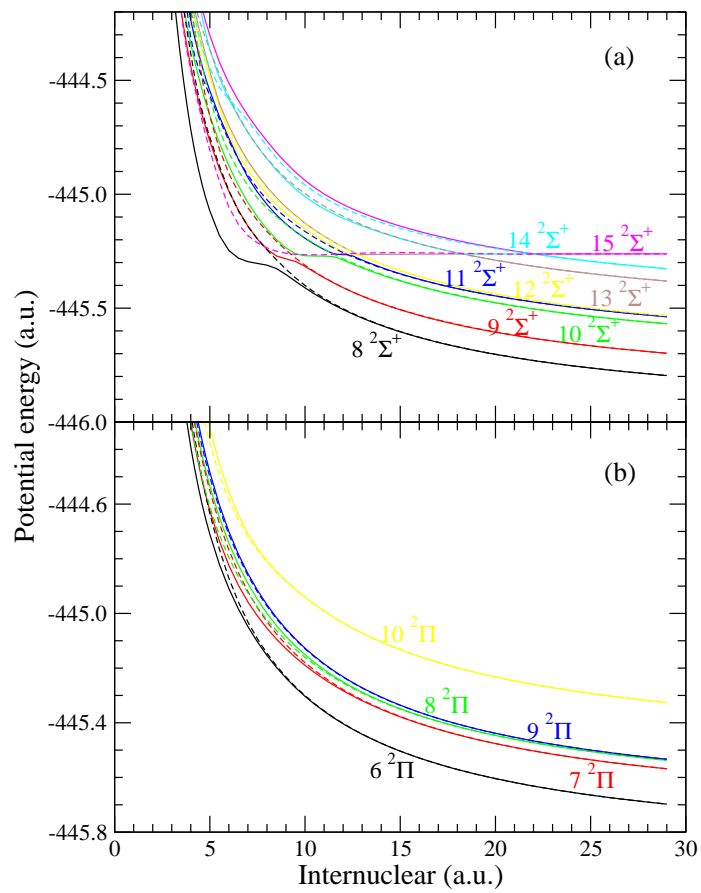


FIG. 1: (Color online) The adiabatic (—) and diagonal diabatic (----) potential energies of the ClH⁷⁺ system as a function of internuclear distance R .

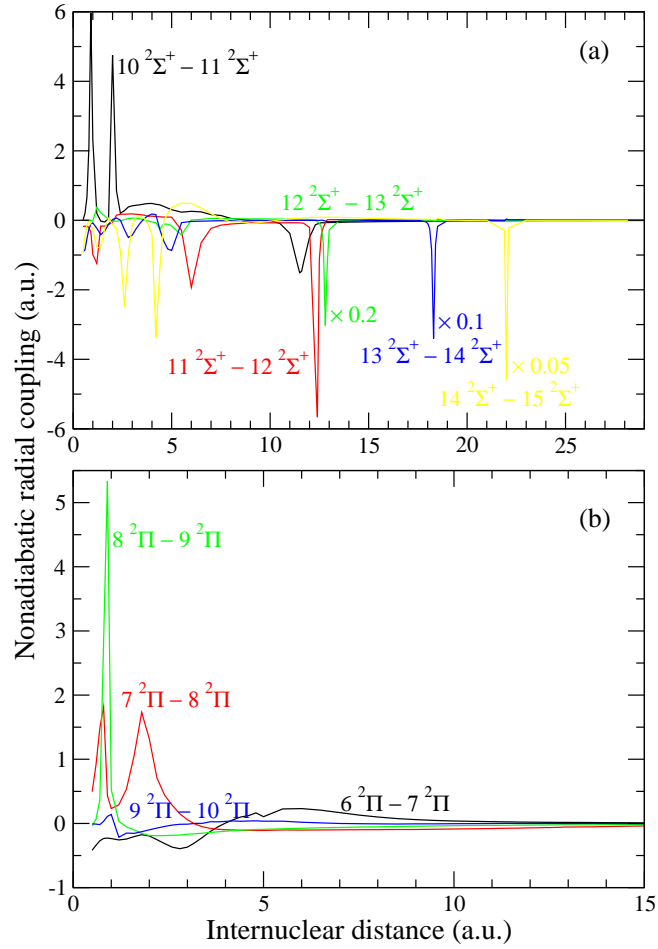


FIG. 2: (Color online) Representative (a) $2\Sigma^+$ and (b) 2Π nonadiabatic radial couplings for the ClH^{7+} system as a function of internuclear distance R . Note that the peak values of some couplings in (a) have been multiplied by a constant.

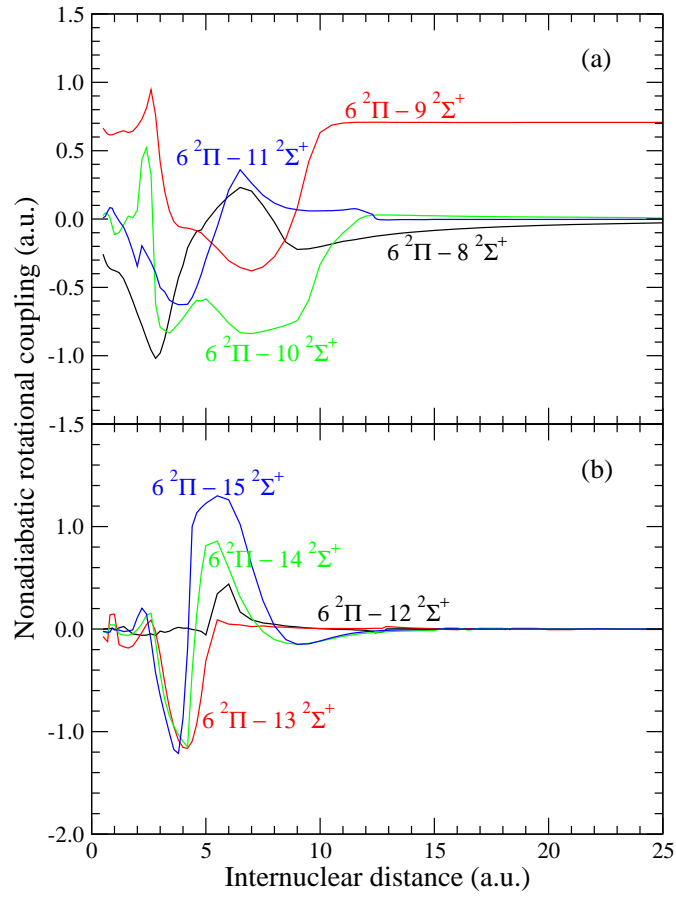


FIG. 3: (Color online) Representative nonadiabatic rotational couplings between the ${}^2\Pi$ and ${}^2\Sigma^+$ states of the ClH^{7+} system as a function of internuclear distance R .

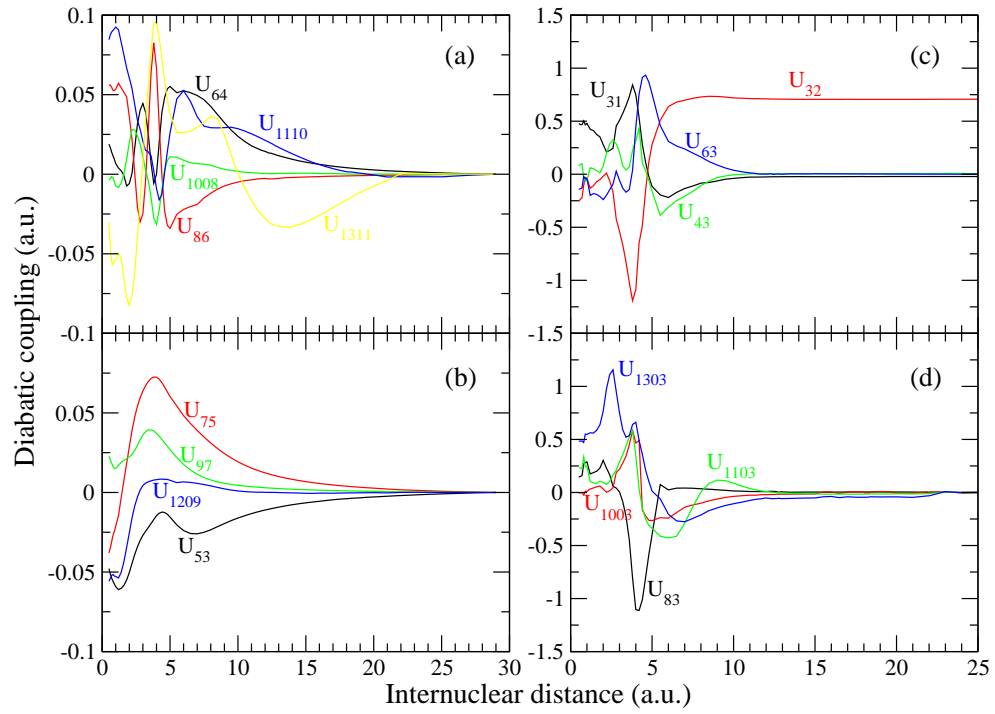


FIG. 4: (Color online) Representative off-diagonal diabatic potentials of CIH^{7+} system as a function of internuclear distance R .

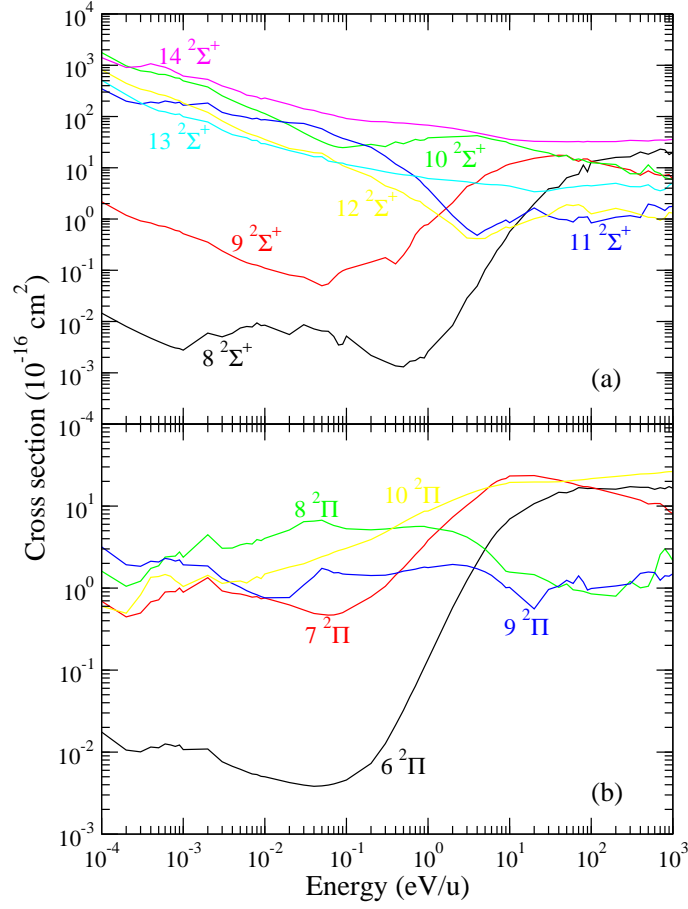


FIG. 5: (Color online) State-to-state QMOCC electron capture cross sections for the ClH⁷⁺ system as a function of relative collision energy E . (a) and (b) correspond to transitions from the entrance channels to all the seven $2\Sigma^+$ states and five 2Π states, respectively.

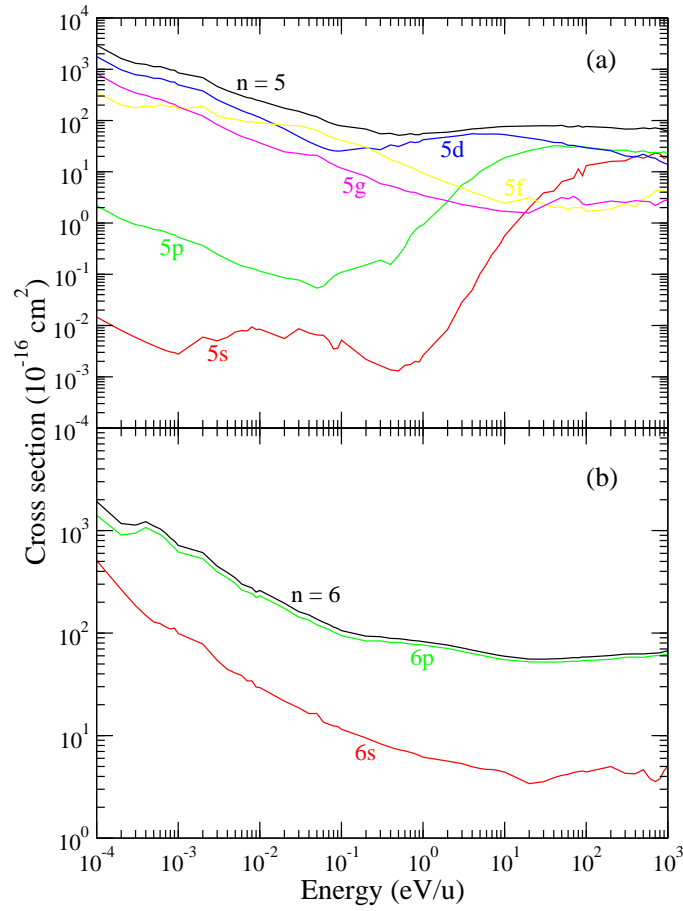


FIG. 6: (Color online) State-selective electron capture cross sections as a function of relative collision energy E . (a) and (b) correspond to capture into $\text{Cl}^{6+}(2p^6 5\ell)$ and $\text{Cl}^{6+}(2p^6 6\ell)$.

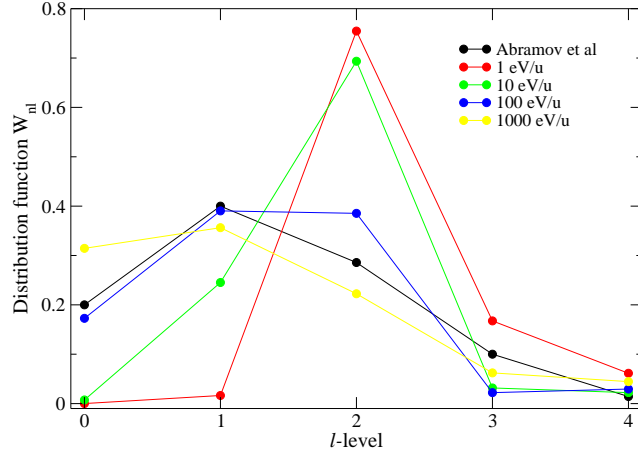


FIG. 7: (Color online) Comparison of ℓ -distributions for the charge-transfer reaction $\text{Cl}^{7+} + \text{H} \rightarrow \text{Cl}^{6+}(2p^6n\ell \ n = 5) + \text{H}^+$ between the calculation from Eq. (9) and the QMOCC results at 1, 10, 100, and 1000 eV/u.

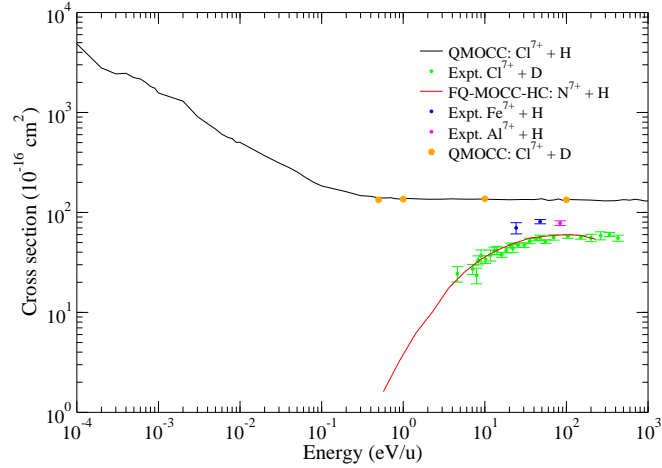


FIG. 8: (Color online) Total electron capture cross sections as a function of relative collision energy E . A comparison is shown with the measurements for the $\text{Cl}^{7+} + \text{D}$ [13], $\text{Fe}^{7+} + \text{H}$ [14] and $\text{Al}^{7+} + \text{H}$ [15] systems and with the fully quantal molecular-orbital close-coupling hidden-crossing calculation (FQ-MOCC-HC) for $\text{N}^{7+} + \text{D}$ system [13]. $\text{Cl}^{7+} + \text{D}$ QMOCC results are also given.